SUPPLEMENTARY DATA

Impact of functional studies on interpretation of exome sequence variants in patients with early-onset cardiac conduction-system diseases

Kenshi Hayashi, Ryota Teramoto, Akihiro Nomura, Yoshihiro Asano, Manu Beerens, Yasutaka Kurata, Isao Kobayashi, Noboru Fujino, Hiroshi Furusho, Kenji Sakata, Kenji Onoue, David Y. Chiang, Tuomas O. Kiviniemi, Eva Buys, Patrick Sips, Micah L. Burch, Yanbin Zhao, Amy E. Kelly, Masanobu Namura, Yoshihito Kita, Taketsugu Tsuchiya, Bunji Kaku, Kotaro Oe, Yuko Takeda, Tetsuo Konno, Masaru Inoue, Takashi Fujita, Takeshi Kato, Akira Funada, Hayato Tada, Akihiko Hodatsu, Chiaki Nakanishi,
Yuichiro Sakamoto, Toyonobu Tsuda, Yoji Nagata, Yoshihiro Tanaka, Hirofumi Okada, Keiich Usuda, Shihe Cui, Yoshihiko Saito, Calum A MacRae, Seiji Takashima, Masakazu Yamagishi, Masa-aki Kawashiri, and Masayuki Takamura.

Supplementary methods

Study patients

The study conformed with the principles outlined in the Declaration of Helsinki and was approved by the Ethics Committee for Medical Research at our institution. All study patients provided written informed consent before registration.

The study patients were recruited from multiple hospitals in Japan. Early-onset cardiac conduction system disease (CCSD) was defined as bradyarrhythmia occurring in individuals aged <65 years, who showed an atrioventricular (AV) block and/or a sick sinus syndrome (SSS) with pacemaker implantation (PMI) or a family history of PMI. AV block was defined as one of the following conditions: (1) every atrial impulse conducted to the ventricles, regular rate, but the PR interval exceeds 0.20 s (first-degree AV block), (2) blocking of some atrial impulses conducted to the ventricle at a time when physiological interference is not involved (second-degree AV block), or (3) no atrial activity is conducted to the ventricles (third-degree AV block). Sick sinus syndrome was defined as one of the following conditions: (1) persistent spontaneous sinus bradycardia not caused by drugs and inappropriate for the physiological circumstance, (2) sinus arrest or exit block, (3) combinations of sinoatrial (SA) and AV conduction disturbances, or (4) alternation of paroxysms of rapid regular or irregular atrial tachyarrhythmias and periods of slow atrial and ventricular rates. In addition, we used the DNA sequencing data of 102 control subjects without electrocardiogram abnormality.

Whole-exome DNA sequencing and determining pathogenicity of candidate variants

Genomic DNA was extracted from peripheral blood leukocytes by using standard methods[1]. Five micrograms of genomic DNA of the patients was submitted to TAKARA BIO INC. (Kusatsu, Shiga, Japan) for whole-exome sequencing (WES). Exome capture was completed with SureSelect Human All Exon V5 + mtDNA (Agilent, Santa Clara, CA, USA). Exome sequencing was performed using the Illumina HiSeq (Illumina, San Diego, CA, USA).

The variants in 117 candidate genes linked to monogenic arrhythmogenic disorders or cardiomyopathies (Supplemental Table 1). We used the Borrows–Wheeler Aligner Maximal Exact Match algorithm to align sequencing reads to human reference genome (build 37). We also used the Genome Analysis Toolkit (GATK ver.3.6) to perform reads' realignments and base quality recalibrations. We set the sensitivity of the Variant Quality Score Recalibration threshold as 99.6% and 95% for single nucleotide variants and insertions/deletions, respectively. We selected protein-truncating variants (PTVs) and rare missense variants. Rare variants were defined as those with minor allele frequency <0.1% in East Asian at the Genome Aggregation Database (gnomAD) version 2.0.2. After the above standard quality control, we selected only the variants that were absent in the in-house WES data from 102 control individuals without early-onset CCSD.

All variants were annotated by the Variant Effect Predictor version 82 and referred following *in silico* damaging scores: MetaSVM for missense variants; LOFTEE for PTVs; and CADD for all variants.[2] MetaSVM score incorporated 10 scores (SIFT, PolyPhen-2 HDIV, PolyPhen-2 HVAR, GERP++, MutationTaster-2, Mutation Assessor, FATHMM, LRT, SiPhy, PhyloP) and the maximum frequency observed in 1000 genome populations. We used the MetaSVM scores from dbNSFP ver.2.9.1. [3] We set the CADD score ≥ 15 as damaging.

We interpreted the sequence variants using 2015 ACMG standards and guidelines, which provided criteria for the classification of pathogenic or likely pathogenic variants.[4] In brief, each pathogenic criterion is weighted as very strong (PVS1), strong (PS1–4), moderate (PM1–6), or supporting (PP1–5). Variants which were absent in East Asian at the Human Genetic Variation Database (HGVD) version 2.3 and gnomAD were considered as PM2. PTVs in known genes associated with CCSD were considered as PVS1, and rare missense variants registered as pathogenic or disease-causing mutation associated with CCSD in disease database including ClinVar or Human Gene Mutation Database were considered as PP5. When multiple lines of in silico prediction algorithms (MetaSVM, LOFTEE, and CADD) supported a deleterious effect on the gene, the supporting pathogenic evidence of PP3 was assigned. We further sought to determine the relationship between the clinical phenotype (bradyarrhythmia) and the genotype for probands and their relatives in whom a variant was identified (PP1 or PP4). These segregation analyses were

performed in the family members as much as possible. If the missense variants are common causes of the disorder and the gene also has very few benign variants, then a missense variant in this gene can be supporting evidence for pathogenicity (PP2). Functional studies were performed using cellular electrophysiological analysis, mathematical modeling, and simulations, and CRISPR/Cas9 mediated gene knock-out in zebrafish to confirm the pathogenicity of detected variants (PS3 or BS3). For a given variant, we selected the criteria based on the evidence observed for the variant. The criteria then are combined according to the scoring rules to choose a classification from the five-tier system (Figure 1).[4]

***in vivo* zebrafish cardiac assay**

All zebrafish experiments have been approved by Institutional Animal Care and Use Committee (protocol# BWH 2016N000276), which is certified by the Association for Assessment and Accreditation of Laboratory Animal Care, and the Bioethical Committee on Medical Research, School of Medicine, Kanazawa University. The procedures were also performed in conformity with the National Institutes of Health (NIH) Guide for the Care and Use of Laboratory Animals (NIH Pub. No. 85-23, Revised 1996). Zebrafish euthanasia was performed following NIH (https://oacu.oir.nih.gov/animal-research-advisory-committee-guidelines) and American Veterinary Medical Association guidelines using an overdose of Tricaine (M-222 or 3-aminobenzoic acid ethyl ester) in combination with hypothermic shock. Transgenic line of zebrafish carring cmlc2:Mermaid was obtained from Dr. Shin-ich Higashijima and Dr. Hidekazu Tsutsui (The National Institutes of Natural Sciences).[5] Transgenic line of zebrafish carring cmlc2::GFP was obtained from Dr. Huai-Jen Tsai (Institute of Molecular and Cellular Biology, National Taiwan University).

The gene editing in zebrafish with CRISPR/Cas9 was conducted to evaluate detected PTV in *LMNA* or *EMD* from patients with early-onset CCSD. The target site of the human *LMNA* ortholog, *lmna*, in zebrafish was selected using a CHOPCHOP webtool, which ranks target sites based on potential off-target effects (5'-GGAGCTCAGCAAAGTGCGTG-3'). Single guide (sg) RNA was generated by in vitro transcription from oligonucleotide-based templates with a MEGAshortscript™ T7 Transcription Kit (Thermo Fisher Scientific Inc., Waltham, MA, USA). DNA double-strand breaks (DSBs) introduced by CRISPR at the target site can be repaired through error-prone nonhomologous end-joining (NHEJ) pathway. The DSB repair by NHEJ could generate indel mutations, which can cause frame shift and then abolish gene function if the mutations occur in an exon. Two microliters of sgRNA stock (400 ng/μl) was mixed with 2 μl of recombinant Cas9 protein (1 μg/μl) (PNA Bio, Newbury Park, CA, USA) and 2μl of water, then incubated on ice for 5 min to allow formation of the sgRNA/Cas9 complex. One nanoliter of the injection mix was injected intracellularly in one-cell

stage zebrafish embryos by using glass needles and a micromanipulator. Zebrafish embryos were maintained in E3 water at 28°C.

To generate mutant lines for evaluating the F0 generation, we also used a rapid knockout method, known as acute CRISPR (aCRISPR). We designed four guide RNAs for the *lmna* exon 6 and *emd* exon 8, respectively. Then, we injected these guide RNAs and CAS9 protein in one-cell stage zebrafish embryos. Multiple guide RNAs for a specific target lesion leads to nearly complete gene disruption.[6] The sequences of the guide RNAs were as followed.

lmna, exon 6:

5'-TGAACAGTTGGCTGCTCGAG-3'

5'-TATTTTGCGCCGTCGTCTGG-3'

5'-GCGCAAAATATCCCTCTCTC-3'

5'-GGATATTTTGCGCCGTCGTC-3'

emd, exon 8:

5'-ACCAGGATGCGCAGCCACGC-3'

5'-GCCGGCGTGGCTGCGCATCC-3'

5'-TGGACGAGAAGAGCTCTGAT-3'

5'-AGTCTGCAGGTGTGCCGGCG-3'

We synthesized CRISPR ribonucleoprotein from four CRISPR RNAs (0.5 µL of each 100 µM, total 2 µL) with 2 µL of tracrRNA (100 µM) and CAS9 proteins (3 µM).

Cardiac phenotypes were scored at 48 and 72 hpf, and genomic DNA was prepared from 10 individuals for Sanger sequencing. The heart rate was visually counted at 48 hpf by using a stereomicroscope. Cardiac function was evaluated at 48 hpf by using video microscopy with an Axioplan (Zeiss) upright microscope. 816 flames (magnification, 10×; frame rate, 250/s) were captured, and sequential still frames were analyzed by Image J. Voltage mapping was recorded on isolated 72 hpf zebrafish hearts [7]. Dissected hearts were stained with FluoVolt (Thermo Fisher Scientific Inc., Waltham, MA, USA) and immobilized with Blebbistatin or Cytochalasin D (Sigma-Aldrich, St. Louis, MO, USA) for the measurement of action potentials. Fluorescence intensities were recorded with a high-speed charge coupled-device camera (RedShirtImaging, Decatur, GA, USA). Acquired fluorescence images were exported as tiff stacks and analyzed using Matlab software (Mathworks, Natick, MA, USA). *In vivo* natriuretic peptide reporter assay on *nppb*:F-Luc embryos at 72 hpf was conducted to evaluate the expression levels of the cardiac natriuretic peptide B which was encoded by *nppb* gene, and highly conserved biomarker of cardiomyocyte dysfunction and hypertrophy. CRISPR/Cas9 or tracrRNA-injected nppb:F-Luc embryos were placed into a 96-well microtiter plate with 100 µL of long half-life firefly luciferase reagent (Perkin Elmer, Steady-Glo).

The plate was then incubated in the dark for 45 min. After 45 min, the plate was read in a high-sensitivity luminescence plate reader (PE Elmer Victor X). The luminescence values obtained between different readers were calibrated to use the same scale. [8]

Mosaic founders (F0) were raised and outcrossed to a wild-type (WT) line at the age of 3 months. Sequencing analysis of F1 fish after outcross was performed at the age of 5 months, and various truncating indels of *lmna* were confirmed. Heterozygous F1 generation fishes were sequenced to identify those with same *lmna* mutation and without having plausible off-targets which were determined by using guide RNA design checker (Integrated DNA Technologies, Coralville, IA). Then they were incrossed, and cardiac phenotypes for F2 embryos were evaluated as stated above. Each F2 embryo was genotyped after evaluation of the cardiac phenotype to distinguish between heterozygous and homozygous carriers. Nuclear structure of cardiomyocytes in WT *lmna* $^{+/+}$ and homozygous *lmna* $^{del/del}$ adult zebrafish was evaluated using immunohistochemistry and confocal microscopy. Adult zebrafish (3 months old) with *lmna*$^{del/del}$ or *lmna*$^{+/+}$ were sacrificed for the isolation of hearts. Then we fixed the hearts with tissue freezing medium after soaking them in Sucrose. The embed heart specimens were sliced (6 µm) by a cryostat and stained by Anti-LaminB1 (Sigma, produced in Rabbit) overnight at 4°C. Alexa Goat anti-rabbit 488 (Abcam) was dropped on the tissue as a secondary antibody and Phalloidin-647 (Abcam) was used for staining F-actin. Finally, we added DAPI to stain the nucleus and placed a coverslip on the slide. Immunohistochemistry imaging was captured using Olympus FV1200 confocal microscope. Total mRNA was isolated from 15 whole bodies of zebrafish larvae (5 days post fertilization) using TRIzol. iScript Reverse Transcription (Bio-Rad) was used to generate cDNA. The real time PCR program was performed using iTaq Universal SYBR Green (Bio-Rad). The nppb gene expression level was normalized to the expression of the housekeeping gene eef1a by calculation of delta Cp = 2^-[Cp nppb gene - Cp eef1a].

To characterize a human *MYH6* variant, *myh6* ATG-blocking morpholino antisense oligonucleotide targeted against the translational start site of *myh6* (*myh6* ATG-MO; ACTCTGCCATTAAAGCATCACCCAT) (Gene Tools LLC, Philamath, OR) (1 ng/embryo) was injected alone or coinjected with human WT or mutant *MYH6* cRNA (0.4 ng/embryo) at the 1- to 2-cell stage, as described previously[9]. Human WT *MYH6* cDNA cloned into pCS2+ vector was provided by Dr. Naomasa Makita and Taisuke Ishikawa (National Cerebral and Cardiovascular Center). cRNAs of human MYH6 were synthesized using the mMESSAGE mMACHINE™ SP6 Transcription Kit (Thermo Fisher, Waltham, MA). The HR and cardiac function were evaluated at 48 hpf by using a stereomicroscope and video microscopy. Voltage mapping was recorded on isolated 72 hpf zebrafish hearts.

Plasmid constructs and electrophysiology

The *KCNH2* cDNA in the mammalian expression vector pSI, the *SCN5A* cDNA in the pCGI vector [10], *SCN1B* cDNA in the IRGFP vector, and the *SCN10A* cDNA in the pIRES2-EGFP plasmid were kindly provided by Dr. Sabina Kupershmidt and Dr. Dan Roden (Vanderbilt University). Mutant cDNAs were constructed by an overlap extension strategy or using a QuikChange XL Site-Directed Mutagenesis Kit (Agilent Technologies, Santa Clara, CA, USA). With regard to the study of Nav1.5 current, HEK293 cells were transiently transfected with WT *SCN5A* cDNA (0.5 μg), or mutant *SCN5A* cDNA (0.5 μg), using a FuGENE 6 Transfection Reagent (Roche Applied Science, Penzberg, Germany). Cells were cotransfected with the same amount of *SCN1B* cDNA in the IRGFP vector as each sodium channel cDNA. With regard to the studies of Kv11.1 current, CHO-K1 cells were transiently transfected with WT *KCNH2* cDNA (0.5 μg), mutant *KCNH2* cDNA (0.5 μg) or WT + mutant *KCNH2* cDNA (0.5 μg each, 1 μg in total), using a FuGENE 6 Transfection Reagent (Roche Applied Science, Penzberg, Germany). Cells were cotransfected with the same amount of green fluorescent protein (GFP) as each potassium channel cDNA. With regard to the study of Nav1.8 current, ND 7/23 cells were transiently transfected with 3 μg of the cDNA encoding human WT or variant Nav1.8, using an X-tremeGENE 9 DNA Transfection Reagent (Roche Applied Science, Penzberg, Germany). ND 7/23 cells were kindly provided by Dr. Naomasa Makita (National Cerebral and Cardiovascular Center). Cells displaying green fluorescence 48–72 h after transfection were subjected to electrophysiological analysis.

Rapidly-activating delayed-rectifier potassium current (I_{Kr}) and fast sodium current (I_{Na}) were measured the whole-cell patch clamp technique with an amplifier, Axopatch-200B (Molecular Devices, Sunnyvale, CA), at room temperature (23°C-25°C for potassium currents and 20°C–22°C for sodium currents). Electrode resistance ranged from 2 to 4 MΩ and from 0.8 to 1.5 MΩ for potassium and sodium channel recordings, respectively. The voltage clamp protocols are described in the Figures. Data were acquired using pCLAMP software (v. 9; Molecular Devices, Sunnyvale, CA, USA). Data acquisition and analysis were performed using a Digidata 1321 A/D converter and pCLAMP8.2 software (Molecular Devices, Sunnyvale, CA, USA).

While recording potassium currents, the pipette solution (intracellular solution) contained 110 mM KCl, 5 mM K_2ATP, 2 mM $MgCl_2$, 10 mM HEPES, and 5 mM K_4BAPTA at pH 7.2, and the bath solution contained 140 mM NaCl, 5.4 mM KCl, 2 mM $CaCl_2$, 1.0 mM $MgCl_2$, 10 mM HEPES, and 10 mM glucose, adjusted to pH 7.4 with NaOH. While recording Nav1.5 currents, the pipette solution (intracellular solution) contained 10 mM NaF, 110 mM CsF, 20 mM CsCl, 10 mM EGTA, and 10 mM HEPES at pH 7.35 with CsOH. The bath solution contained 145 mM NaCl, 1.5 mM $CaCl_2$, 4.5 mM

KCl, 1 mM $MgCl_2$, 10 mM HEPES, and 5 mM glucose, adjusted to pH 7.4 with CsOH. While recording Nav1.8 currents, the pipette solution (intracellular solution) contained 10 mM NaF, 110 mM CsF, 20 mM CsCl, 5 mM EGTA, 10 mM HEPES, and 5 mM Mg2-ATP, with a pH of 7.3 adjusted with CsOH. The bath solution contained 135 mM NaCl, 1.8 mM CaCl2, 1.0 mM MgCl2, 20 mM TEA-Cl, 10 mM HEPES, and 10 mM glucose, with a pH of 7.4, adjusted with NaOH. Endogenous tetrodotoxin (TTX)-sensitive I_{Na} and L- and T-type calcium currents were eliminated with TTX 200 nM, nisoldipine 1 μM and NiCl2 200 μM, respectively.

The voltage dependence of potassium current activation was determined for each cell by fitting peak values of tail current (I_{tail}) versus test potential to a Boltzmann function in the following form: $I_{tail}=I_{tail\text{-}max}/\ \{1+\exp[(V_{1/2}-V_t)/k]\}$, where $I_{tail\text{-}max}$ is peak I_{tail}, V_t is the test potential, $V_{1/2}$ is the voltage at which I_{tail} is half of $I_{tail\text{-}max}$, and k is the slope factor [11]. Steady-state inactivation of the potassium current was analyzed as previously described[12]. Briefly, the corrected steady-state inactivation curves were fitted with a Boltzmann function in the following form: $I/(I_{ma}-I_{min}) = 1/\ \{1+\exp[(V_t-V_{1/2})/k]\}\ + I_{min}$, where I is the amplitude of the inactivating current corrected for deactivation, I_{max} is the maximum of I, I_{min} is the minimum of I, V_t is the prepulse of test potential, $V_{1/2}$ is the voltage at which I is half of I_{max}, and k is the slope factor. Deactivation rates of Kv11.1 channels were measured using a two-step voltage protocol and by fitting tail currents with two exponential functions [11].

The parameters for voltage dependence of sodium current activation were estimated from the current–voltage relationship based on the Boltzmann equation in the following form: $I = G_{max} \times (V - V_{rev}) \times (1 + \exp[V - V_{1/2}]/k)^{-1}$, where I is the peak Na current during the test pulse potential V. The parameters estimated by the fitting are G_{max} (maximum conductance), V_{rev} (reversal potential), and k (slope factor) [13]. Steady-state availability for fast inactivation was measured with a standard double-pulse protocol, and the data were fit with the Boltzmann equation in the following form: $I/I_{max} = (1 + \exp[(V - V_{1/2})/k])^{-1}$, where I_{max} is the maximum peak Na current, to determine the membrane potential for $V_{1/2}$ and k [13].

Simulations of cardiac action potentials

With mathematical models of human ventricular myocytes [14] and rabbit peripheral sinoatrial node (SAN) cells [15], we evaluated effects of the effects of the changes in kinetic behavior of I_{Kr} and I_{Na} on the mid-myocardial action potential configuration of the ventricular myocyte model and pacemaker activity of the peripheral SAN cell model connected to the atrial membrane model via the gap junction conductance. Dynamic behaviors of the model cell were determined by solving a system of nonlinear ordinary differential equations numerically. Numerical integration was performed on

Workstation HP xw9400 with MATLAB 7.5 (The MathWorks, Inc., Natick, MA, USA). The numerical algorithms available as a MATLAB ODE solver, *ode15s* (a variable time-step numerical differentiation approach selected for its suitability to stiff systems) were used.

Statistical analysis

Pooled electrophysiological data were expressed as mean±standard error. Two-tailed Student's *t*-test was used for single comparisons between two groups. One-way ANOVA, followed by a Bonferroni *post hoc* test, was used to analyze data with equal variance among three or more groups. A value of $P<0.05$ was considered statistically significant. Statistical analysis was performed using JMP Pro 11.0.0 (SAS Institute Inc., NC, USA) and Origin 2018 (OriginLab, Northampton, MA, USA).

Supplementary figure Legends

Figure S1. Generation of patient-specific mutant lines in zebrafish using CRISPR-mediated deletions of the human *LMNA* or *EMD* ortholog, *lmna* or *emd*, in zebrafish.

Figure S2. Functional studies of PTV, *LMNA* c.339dupT using CRISPR-mediated deletions of the human *LMNA* ortholog, *lmna*, in zebrafish .

(A) Representative images illustrating the morphology of sgRNA injected and sgRNA/Cas9 injected embryos at 48 hpf and Sanger sequence of *lmna* gene. (B) Heart rate of non-injected embryos (n=61), sgRNA injected embryos (n=37), and sgRNA/Cas9 injected embryos (n=66). $^{\dagger}P<0.01$. (C) Isochronal map of sgRNA injected and sgRNA/Cas9 injected embryos summarizing the regional spread of electrical activity across the atrium and into the ventricle. The lines represent the positions of the action potential wavefront at 5-ms intervals. Mean estimated conduction velocities of ventricle from sgRNA injected and sgRNA/Cas9 injected embryos with indels of *lmna*. $^{\dagger}P<0.01$; PAM, protospacer adjacent motif.

Figure S3. Sequencing analysis of *lmna* for F1 fish after outcross between mosaic founders (F0) and wild-type (WT) fishes.

For detection of deletion or insertion mutations, Sanger sequence was performed by the usual method (left) and after treatment of TA cloning, using the TOPO TA cloning kit (Thermo Fisher, Waltham, MA) (right).

Figure S4. Sequencing analysis of potential off-target site in *herc1* for F1 fish.

(A) Guide RNA design checker determined the potential off-target site in the *herc1*, to which 2 mismatches in the gRNA design were compared. (B) Sanger sequences of the potential off-target site in the *herc1* for F1 fishes after outcross between mosaic founders (F0) and wild-type (WT) fishes.

Figure S5. Immunohistochemistry and RT-qPCR analysis of gene expression in *lmna* mutant zebrafish

(A) Representative confocal images of control and mutant zebrafish hearts. Cardiomyocytes in the atrium and ventricle were stained with an antibody against LaminB1 (green). Blue, 4',6-diamidino-2-phenylindole (DAPI). Gray, Phalloidin-647. (B) Relative mRNA expression of the *nppb* gene in control and mutant zebrafish whole body. $^{\dagger}P<0.01$.

Figure S6. Functional studies of PTV, *LMNA* p.R321X using CRISPR-mediated deletions of the human *LMNA* ortholog, *lmna*, in zebrafish.

(A) Multiple sequence alignment of human *LMNA* and zebrafish *lmna*. PAM, protospacer adjacent motif: DSB, double strand break. (B) Representative images illustrating the morphology of 2 dpf tracrRNA-injected and *lmna* exon6 aCRISPR embryos and Sanger sequence of *lmna* gene. (C) Heart rate of tracrRNA-injected (n=18) and *lmna* exon6 aCRIPR (n=22) embryos. (D) Cardiac output of tracrRNA injected (n=18) and *lmna* exon6 aCRIPR (n=22) embryos. (E) Isochronal map of tracr-RNA and *lmna* exon6 aCRIPR injected embryos summarizing the regional spread of electrical activity across the atrium and into the ventricle. (F) Mean estimated conduction velocities at the atrium, AV canal, and ventricle of tracrRNA-injected (n=7) and *lmna* exon 6 aCRIPR (n=7) embryos. Regions of interest was placed at middle of atrium, AV canal or ventricle. $^{\dagger}p<0.01$.

Figure S7. In vivo natriuretic peptide reporter assay on CRISPR/Cas9 or tracrRNA-injected nppb:F-Luc embryos at 72 hpf.

(A) Comparison of expression of the luciferase transgene between tracrRNA-injected and *lmna* exon6 aCRISPR embryos. (B) Comparison of expression of the luciferase transgene between tracrRNA-injected and *emd* aCRISPR embryos.

Figure S8. The functional consequence of *SCN10A* F507L variant assessed by whole-cell patch clamp recording

(A) The voltage protocol and representative current traces of Na_v 1.8 using wild-type and mutant channel. (B) I–V relationships for peak currents in ND 7/23 cells transfected with *SCN10A* WT (n=9) and F507L variant (n=18). The maximum peak current density of F507L was −82.9 ± 14.3 pA/pF, which was comparable to −94.2 ± 18.0 pA/pF for WT. (C) Normalized steady-state activation curves of *SCN10A* WT (n=7) and F507L variant (n=14). The voltage dependence of steady-state activation of F507L was similar to that of WT. (D) The voltage protocols and normalized steady-state inactivation curves of *SCN10A* WT (n=15) and F507L variant (n=15). The voltage dependence of steady-state inactivation of F507L was similar to that of WT.

Figure S9. Functional study of *MYH6* p.R1252Q using targeted zebrafish *myh6* knockdown and overexpressed human *MYH6* in zebrafish.

(A) Representative images illustrating the morphology of embryonic zebrafish at 48hpf: non-injected control, *myh6* MO-injected, *myh6* MO co-injected with human *MYH6* WT cRNA (*myh6* MO+*MYH6* WT), and *myh6* MO co-injected with human *MYH6* R1252Q cRNA (*myh*6 MO+*MYH6* R1252Q). (B)

Heart rate of embryonic zebrafish at 48hpf: non-injected control (n=75), *myh6* MO-injected (n=73), *myh6* MO+*MYH6* WT (n=69), and *myh*6 MO+*MYH6* R1252Q (n=70). (C) and (D) Stroke volume and cardiac output of embryonic zebrafish at 48hpf: non-injected control (n=24), *myh6* MO-injected (n=21), *myh6* MO+*MYH6* WT (n=24), and *myh*6 MO+*MYH6* R1252Q (n=24). (E) Mean conduction velocities at the ventricle of embryonic zebrafish at 72hpf: non-injected control (n=3), *myh6* MO-injected (n=5), *myh6* MO+*MYH6* WT (n=4), and *myh*6 MO+*MYH6* R1252Q (n=5). MO, morpholino oligonucleotide; $^{\dagger}P<0.01$; $^{*}P<0.05$.

Supplementary References

1. Nomura A, Tada H, Teramoto R, Konno T, Hodatsu A, Won HH, Kathiresan S, Ino H, Fujino N, Yamagishi M, Hayashi K. Whole exome sequencing combined with integrated variant annotation prediction identifies a causative myosin essential light chain variant in hypertrophic cardiomyopathy. *J Cardiol*. 2016;67:133-139.
2. McLaren W, Pritchard B, Rios D, Chen Y, Flicek P, Cunningham F. Deriving the consequences of genomic variants with the Ensembl API and SNP Effect Predictor. *Bioinformatics*. 2010;26:2069-2070.
3. Liu X, Jian X, Boerwinkle E. dbNSFP v2.0: a database of human non-synonymous SNVs and their functional predictions and annotations. *Hum Mutat*. 2013;34:E2393-2402.
4. Richards S, Aziz N, Bale S, Bick D, Das S, Gastier-Foster J, Grody WW, Hegde M, Lyon E, Spector E, Voelkerding K, Rehm HL, Committee ALQA. Standards and guidelines for the interpretation of sequence variants: a joint consensus recommendation of the American College of Medical Genetics and Genomics and the Association for Molecular Pathology. *Genet Med*. 2015;17:405-424.
5. Tsutsui H, Higashijima S, Miyawaki A, Okamura Y. Visualizing voltage dynamics in zebrafish heart. *J Physiol*. 2010;588:2017-2021.
6. Wu RS, Lam, II, Clay H, Duong DN, Deo RC, Coughlin SR. A Rapid Method for Directed Gene Knockout for Screening in G0 Zebrafish. *Dev Cell*. 2018;46:112-125 e114.
7. Panakova D, Werdich AA, Macrae CA. Wnt11 patterns a myocardial electrical gradient through regulation of the L-type Ca(2+) channel. *Nature*. 2010;466:874-878.
8. Becker JR, Robinson TY, Sachidanandan C, Kelly AE, Coy S, Peterson RT, MacRae CA. In vivo natriuretic peptide reporter assay identifies chemical modifiers of hypertrophic cardiomyopathy signalling. *Cardiovasc Res*. 2012;93:463-470.
9. Ishikawa T, Jou CJ, Nogami A, Kowase S, Arrington CB, Barnett SM, Harrell DT, Arimura T, Tsuji Y, Kimura A, Makita N. Novel mutation in the alpha-myosin heavy chain gene is associated with sick sinus syndrome. *Circ Arrhythm Electrophysiol*. 2015;8:400-408.
10. Fukuda K, Davies SS, Nakajima T, Ong BH, Kupershmidt S, Fessel J, Amarnath V, Anderson ME, Boyden PA, Viswanathan PC, Roberts LJ, 2nd, Balser JR. Oxidative mediated lipid peroxidation recapitulates proarrhythmic effects on cardiac sodium channels. *Circ Res*. 2005;97:1262-1269.
11. Hayashi K, Shimizu M, Ino H, Yamaguchi M, Mabuchi H, Hoshi N, Higashida H. Characterization of a novel missense mutation E637K in the pore-S6 loop of HERG in a patient with long QT syndrome. *Cardiovasc Res*. 2002;54:67-76.
12. Smith PL, Baukrowitz T, Yellen G. The inward rectification mechanism of the HERG cardiac

potassium channel. *Nature*. 1996;379:833-836.

13. Makita N, Behr E, Shimizu W, et al. The E1784K mutation in SCN5A is associated with mixed clinical phenotype of type 3 long QT syndrome. *J Clin Invest*. 2008;118:2219-2229.
14. Kurata Y, Hisatome I, Matsuda H, Shibamoto T. Dynamical mechanisms of pacemaker generation in IK1-downregulated human ventricular myocytes: insights from bifurcation analyses of a mathematical model. *Biophys J*. 2005;89:2865-2887.
15. Kurata Y, Matsuda H, Hisatome I, Shibamoto T. Regional difference in dynamical property of sinoatrial node pacemaking: role of na+ channel current. *Biophys J*. 2008;95:951-977.

Table S1 CCSD candidate 117 genes linked to arrhythmogenic diseases or cardiomyopathies

ABCC9	*COL3A1*	*ILK*	*MAP2K1*	*PRKAG2*	*TBX5*
ACTA2	*CRYAB*	*JPH2*	*MAP2K2*	*PTPN11*	*TCAP*
ACTC1	*CSRP3*	*JUP*	*MOG1*	*RAF1*	*TGFB3*
ACTN2	*DES*	*KCNA5*	*MYBPC3*	*RBM20*	*TGFBR1*
AKAP9	*DMD*	*KCND3*	*MYH6*	*RYR2*	*TGFBR2*
ANKB	*DMPK*	*KCNE1*	*MYH7*	*SCN10A*	*TMEM43*
ANKRD1	*DSC2*	*KCNE2*	*MYH11*	*SCN1B*	*TMPO*
BAG3	*DSG2*	*KCNE3*	*MYL2*	*SCN2B*	*TNNC1*
BRAF	*DSP*	*KCNE5*	*MYL3*	*SCN3B*	*TNNI3*
CACNA1C	*EMD*	*KCNH2*	*MYLK*	*SCN4B*	*TNNT2*
CACNA2D1	*EYA4*	*KCNJ2*	*MYLK2*	*SCN5A*	*TPM1*
CALM1	*FBN1*	*KCNJ3*	*MYO6*	*SGCD*	*TRDN*
CALM2	*FBN2*	*KCNJ5*	*MYOZ2*	*SHOC2*	*TRPM4*
CALM3	*FXN*	*KCNJ8*	*MYPN*	*SLAMP*	*TTN*
CALR3	*GJA1*	*KCNN2*	*NEXN*	*SLC2A10*	*TTR*
CASQ2	*GJA5*	*KCNQ1*	*NKX2.5*	*SLC8A1*	*TXNRD2*
CAV3	*GLA*	*KRAS*	*NRAS*	*SMAD3*	*VCL*
CBL	*GPD1L*	*LAMP2*	*PDLIM3*	*SNTA1*	
CBS	*HCN4*	*LDB3*	*PKP2*	*SOS1*	
CMK2D	*HRAS*	*LMNA*	*PLN*	*TAZ*	

Table S2 Overview of detected rare variants of patients with early-onset CCSD

Gene	Base change	Amino acid change	gnomAD (East Asian)	HGVD (JPN)	MetaSVM	CADD Score	LOFTEE	Novelty (ClinVar)	Novelty (HGMD)
EMD	677G>A	W226X	NA	NA	NA	39	HC	Not registered	DM for EDMD
	664C>T	Q222X	NA	NA	NA	37	HC	Not registered	Not registered
LMNA	339dupT	K114XfsX1	NA	NA	NA	34	HC	Likely pathogenic	Not registered
	1489-2A>G		NA	NA	NA	24.9	HC	Not registered	DM for cardiac disease
	961C>T	R321X	NA	NA	NA	37	HC	Pathogenic	DM for DCM
KCNH2	805C>T	R269W	NA	NA	D	27.2	NA	Not provided	DM for LQTS+SSS
SCN5A	5470C>G	P1824A	NA	NA	D	24.6	NA	Not provided	DM for LQTS+SSS
SCN10A	3787C>T	R1263X	NA	NA	NA	48	HC	Not registered	Not registered
	4444A>G	I1482V	NA	NA	D	19.0	NA	Not registered	Not registered
	5455G>T	D1819Y	NA	NA	D	31	NA	Not registered	Not registered
	4118T>G	M1373R	NA	NA	D	28.2	NA	Uncertain significance	Not registered
	1519T>C	F507L	NA	NA	D	22.4	NA	Not registered	Not registered
	2413G>A	G805S	NA	NA	D	32	NA	Not registered	Not registered
RYR2	2300C>G	S767W	NA	0.0004	D	34	NA	Not registered	Not registered
MYH6	3347G>A	R1116H	NA	NA	D	28	NA	Uncertain significance	Not registered
	3755G>A	R1252Q	0.000054	0.0004	D	27.3	NA	Not registered	Not registered
MYH7	968T>C	I323T	NA	NA	D	24.1	NA	Uncertain significance	VUS for HCM
MYH11	4532G>A	R1511Q	NA	NA	D	34	NA	Not registered	Not registered
RBM20	3649G>A	G1217R	NA	0.0008	D	28.3	NA	Uncertain significance	Not registered
TTN	70264G>C	G23422R	0.00012	0.0004	D	22.3	NA	Not registered	Not registered
DES	556G>A	D186N	NA	NA	D	24.7	NA	Not registered	Not registered
CBS	1552T>C	Y518H	NA	NA	D	17.9	NA	Not registered	Not registered
TBX5	409G>A	V137M	NA	0.0004	D	32	NA	Not registered	Not registered
ACTC1	710C>T	S237F	NA	NA	D	29.2	NA	Not registered	Not registered
PRKAG2	1366C>G	R456G	0.000058	NA	D	23.7	NA	Not registered	Not registered
MAP2K2	937C>T	R313W	NA	NA	D	27.1	NA	Uncertain significance	Not registered

gnomAD, Genome Aggregation Database; HGVD, Human Genetic Variation Database; MetaSVM, in silico ensemble damaging score; CADD, combined

annotation dependent depletion; LOFTEE, loss-of-function transcript effect estimator; HGMD, human gene mutation database; NA, not available; D, rare damaging variants; HC, high-confidence; DM, disease causing mutation; EDMD, Emery-Dreifuss muscular dystrophy; DCM, dilated cardiomyopathy; LQTS, long QT syndrome, HCM, hypertrophic cardiomyopathy; VUS, variant of unknown significance.

Table S3 The evaluation of cardiac function at 48 hpf and conduction velocity at 72 hpf of the F0 *lmna* exon 6 aCRISPR and tracrRNA- injected embryos

	tracrRNA-injected (control)	*lmna* exon 6 aCRISPR
Cardiac function	n=18	n=22
Heart rate (bpm)	140 ± 9	128 ± 9[†]
Stroke volume (nl)	0.62 ± 0.17	0.72 ± 0.20
Cardiac output (nl/min)	85.68 ± 22.93	91.78 ± 28.09
Fractional area change (%)	38.61 ± 8.81	40.00 ± 7.73
Conduction velocity	n=7	n=7
Atrium (mm/sec)	6.37 ± 2.48	4.55 ± 2.03
Atrioventricular canal (mm/sec)	0.86 ± 0.32	0.78 ± 0.20
Ventricle (mm/sec)	19.26 ± 7.12	7.10 ± 2.74[†]

[†]P<0.01 vs. tracrRNA injected.

Table S4 The evaluation of cardiac function at 48 hpf and conduction velocity at 72 hpf of the embryos with *myh6* MO-injected, *myh6* MO+*MYH6* WT, *myh6* MO+*MYH6* R1252Q, and control

	Non-injected (control)	*myh6* MO-injected	*myh6* MO+*MYH6* WT	*myh6* MO+*MYH6* R1252Q
Heart rate (bpm)	153 ± 13 (n=75)	144 ± 16[†] (n=73)	156 ± 14[*] (n=69)	151 ± 17[‡] (n=70)
Cardiac function	n=24	n=21	n=24	n=24
Stroke volume (nl)	0.83 ± 0.27	0.16 ± 0.09[†]	0.32 ± 0.15[†, ‡]	0.16 ± 0.09[†, §]
Cardiac output (nl/min)	122.22 ± 42.38	22.03 ± 12.30[†]	50.46 ± 23.07[†, *]	24.86 ± 16.44[†, ¶]
Fractional area change (%)	38.34 ± 9.84	23.81 ± 11.22[†]	32.25 ± 8.11	21.25 ± 12.45[†, ¶]
Conduction velocity	n=3	n=5	n=4	n=5
Atrium (mm/sec)	2.92 ± 0.51	3.86 ± 1.29	5.79 ± 2.36	5.64 ± 2.00
Atrioventricular canal (mm/sec)	0.62 ± 0.05	0.67 ± 0.26	1.06 ± 1.18	0.92 ± 0.36
Ventricle (mm/sec)	13.65 ± 3.13	3.93 ± 1.19[†]	8.89 ± 3.92	4.51 ± 2.19[†]

[†]P<0.01 vs. non-injected; [*]P<0.01 vs. *myh6* MO-injected; [‡]P<0.05 vs. *myh6* MO-injected; [§]P<0.05 vs. *myh6* MO+*MYH6* WT; [¶]P<0.01 vs. *myh6* MO+*MYH6* WT.

Figure S1

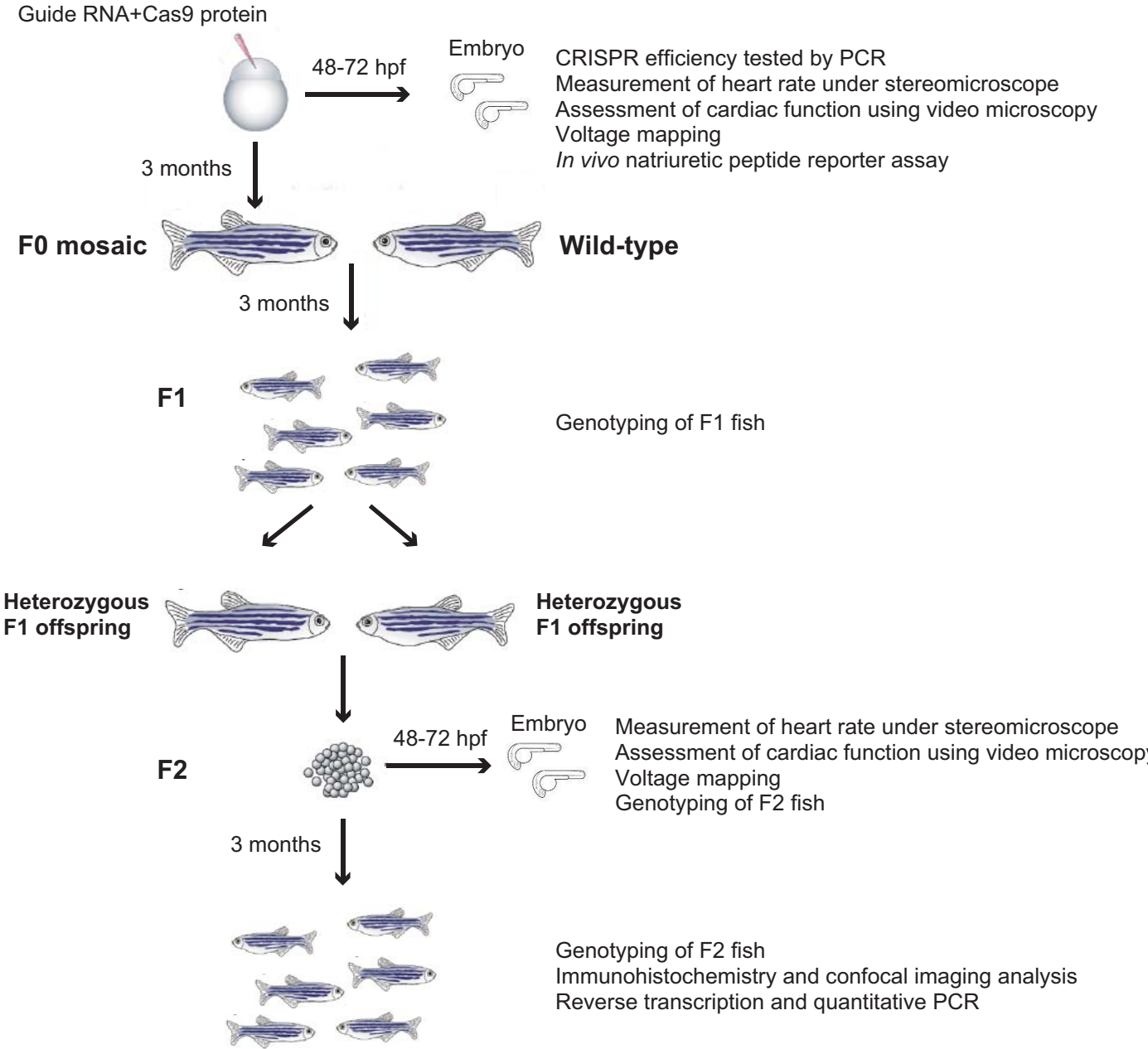
Guide RNA+Cas9 protein
48-72 hpf
Embryo
CRISPR efficiency tested by PCR
Measurement of heart rate under stereomicroscope
Assessment of cardiac function using video microscopy
Voltage mapping
In vivo natriuretic peptide reporter assay
3 months
F0 mosaic
Wild-type
3 months
F1
Genotyping of F1 fish
Heterozygous F1 offspring
Heterozygous F1 offspring
F2
48-72 hpf
Embryo
Measurement of heart rate under stereomicroscope
Assessment of cardiac function using video microscopy
Voltage mapping
Genotyping of F2 fish
3 months
Genotyping of F2 fish
Immunohistochemistry and confocal imaging analysis
Reverse transcription and quantitative PCR

Figure S2

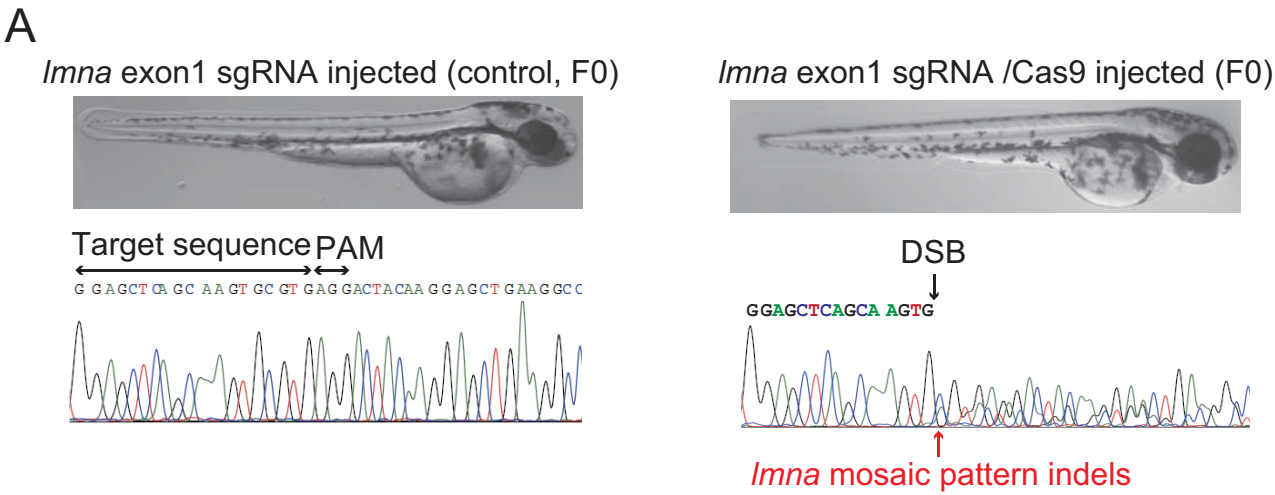
A
lmna exon1 sgRNA injected (control, F0)
lmna exon1 sgRNA /Cas9 injected (F0)
Target sequence
PAM
DSB
GGAGCTCAGCA AGTG
lmna mosaic pattern indels

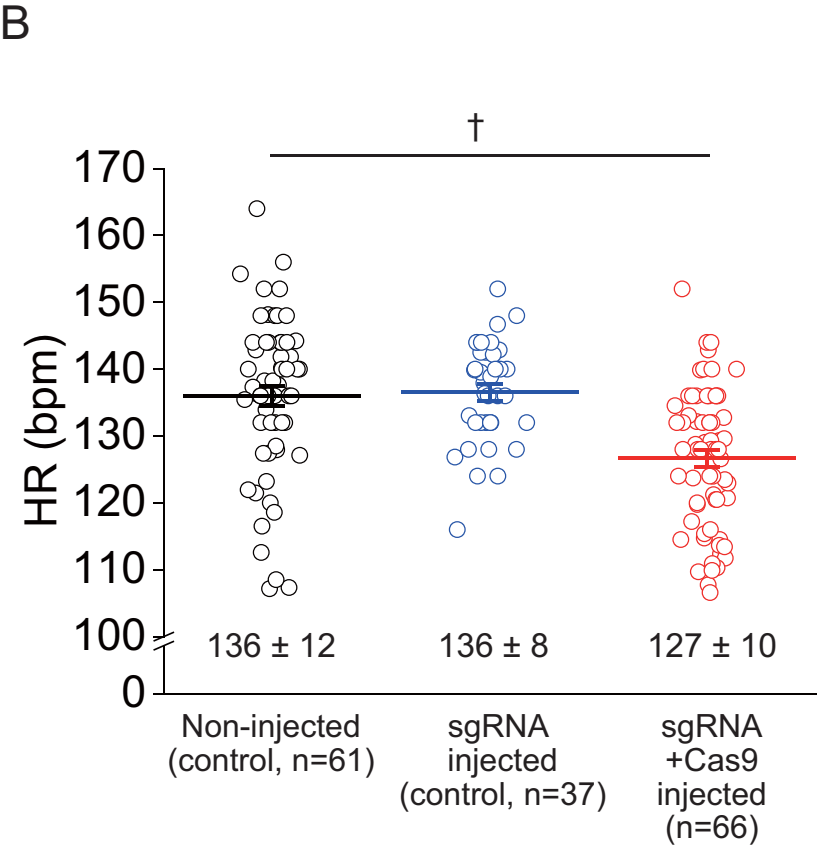
B
HR (bpm)
170
160
150
140
130
120
110
100
0
†
136 ± 12
136 ± 8
127 ± 10
Non-injected (control, n=61)
sgRNA injected (control, n=37)
sgRNA +Cas9 injected (n=66)

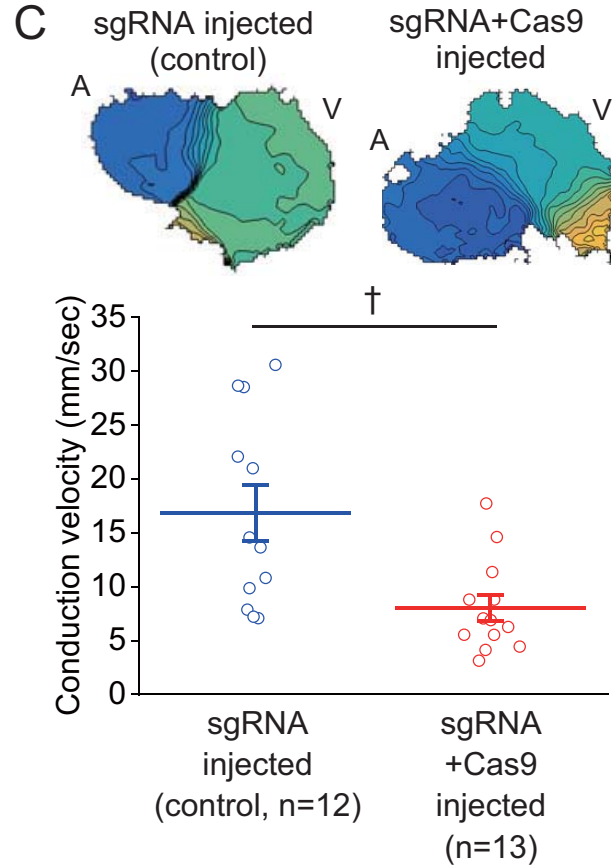
C
sgRNA injected (control)
sgRNA+Cas9 injected
A
V
A
V
Conduction velocity (mm/sec)
35
30
25
20
15
10
5
0
†
sgRNA injected (control, n=12)
sgRNA +Cas9 injected (n=13)

Figure S3

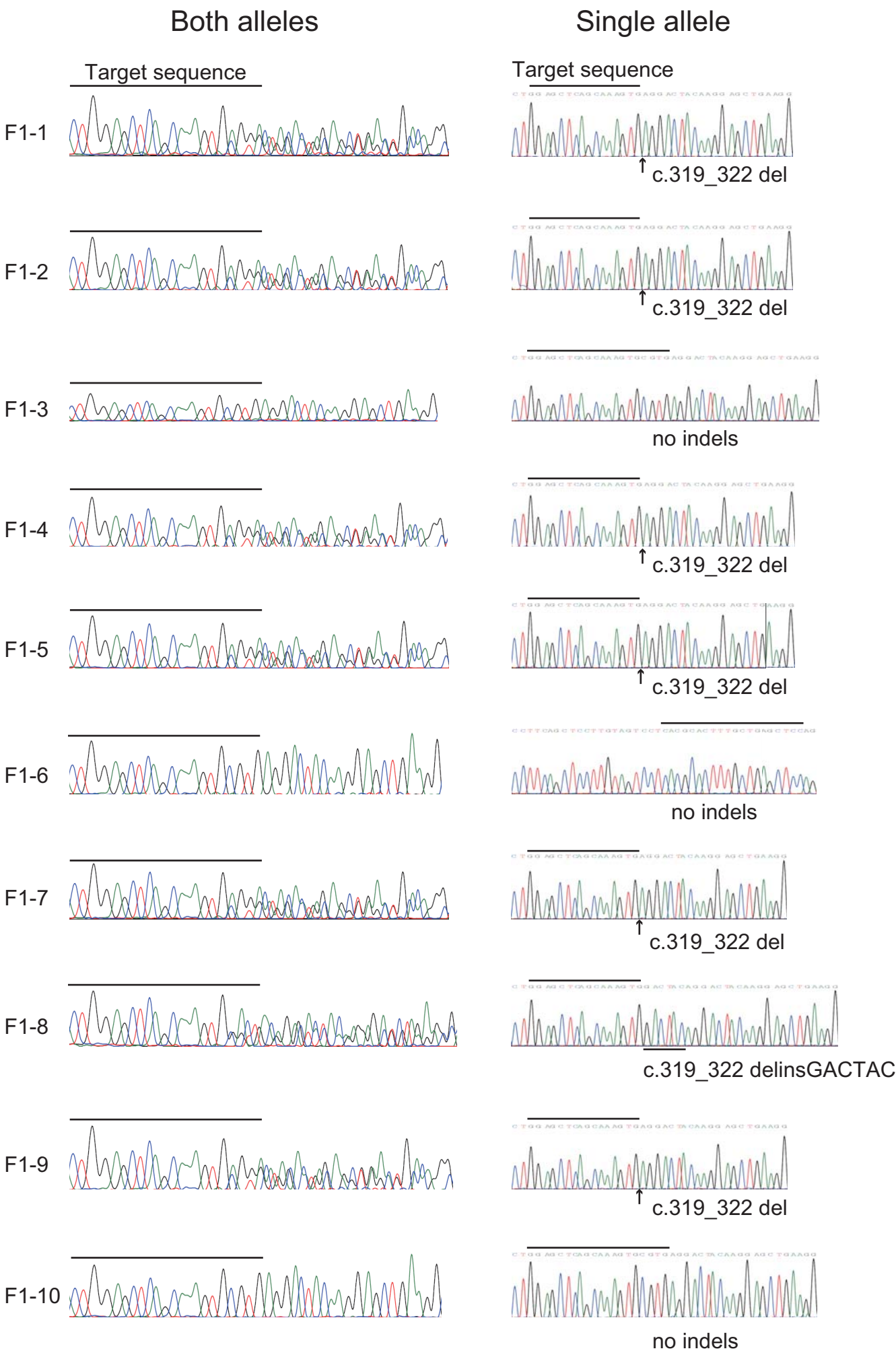
Both alleles
Single allele
Target sequence
Target sequence
F1-1
c.319_322 del
F1-2
c.319_322 del
F1-3
no indels
F1-4
c.319_322 del
F1-5
c.319_322 del
F1-6
no indels
F1-7
c.319_322 del
F1-8
c.319_322 delinsGACTAC
F1-9
c.319_322 del
F1-10
no indels

Figure S4

A

Type of target site	Sequence	PAM	Gene	Locus
Target site for *lmna* gene	GGAGCTCAGCAAAGTGCGTG	AGG	*lmna*	16:-30562785
Potential off-target site	CGAGCT - AGCAAAGTGCGTG	CAG	*herc1*	17:+29223503

B

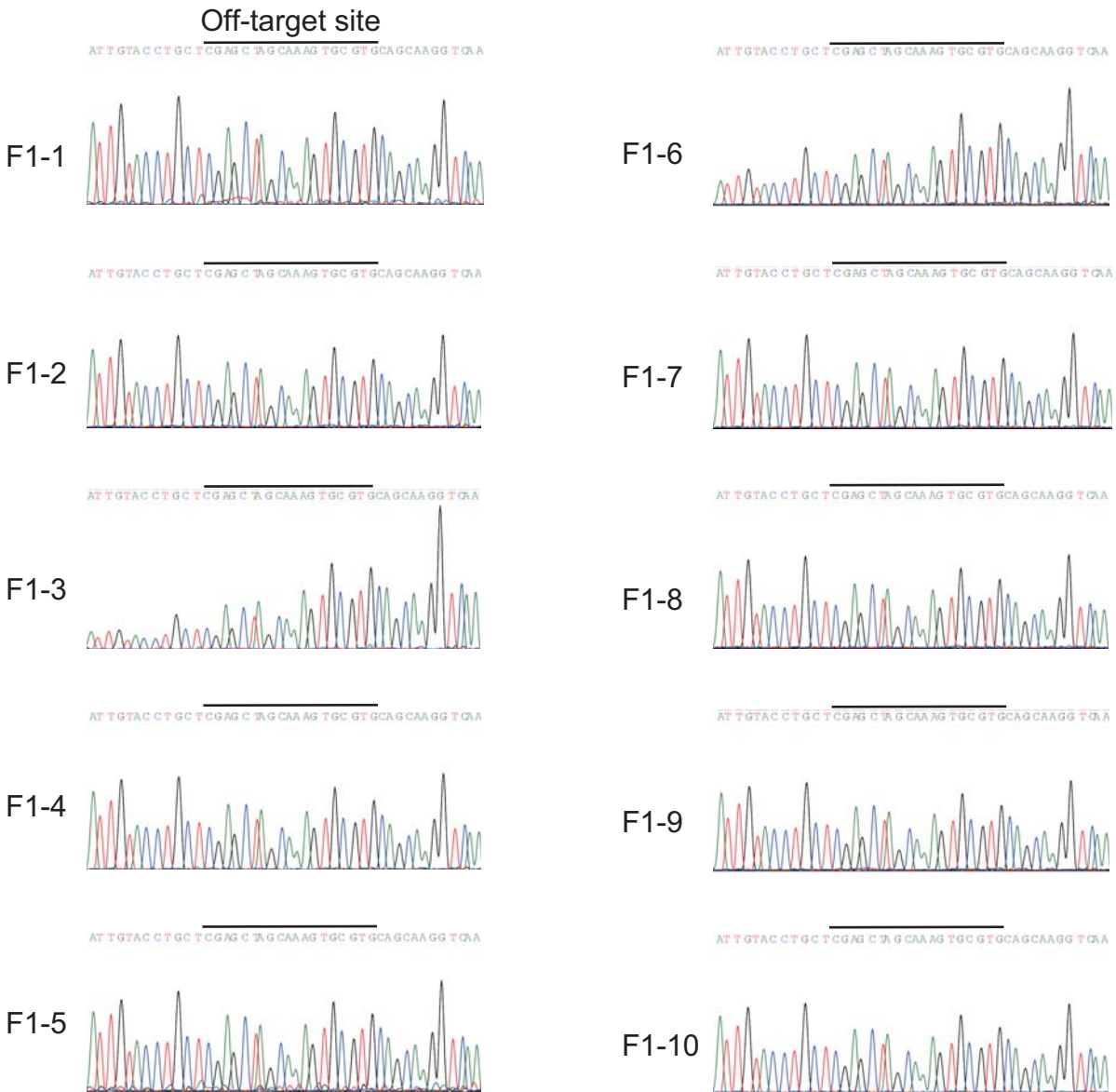

Figure S5

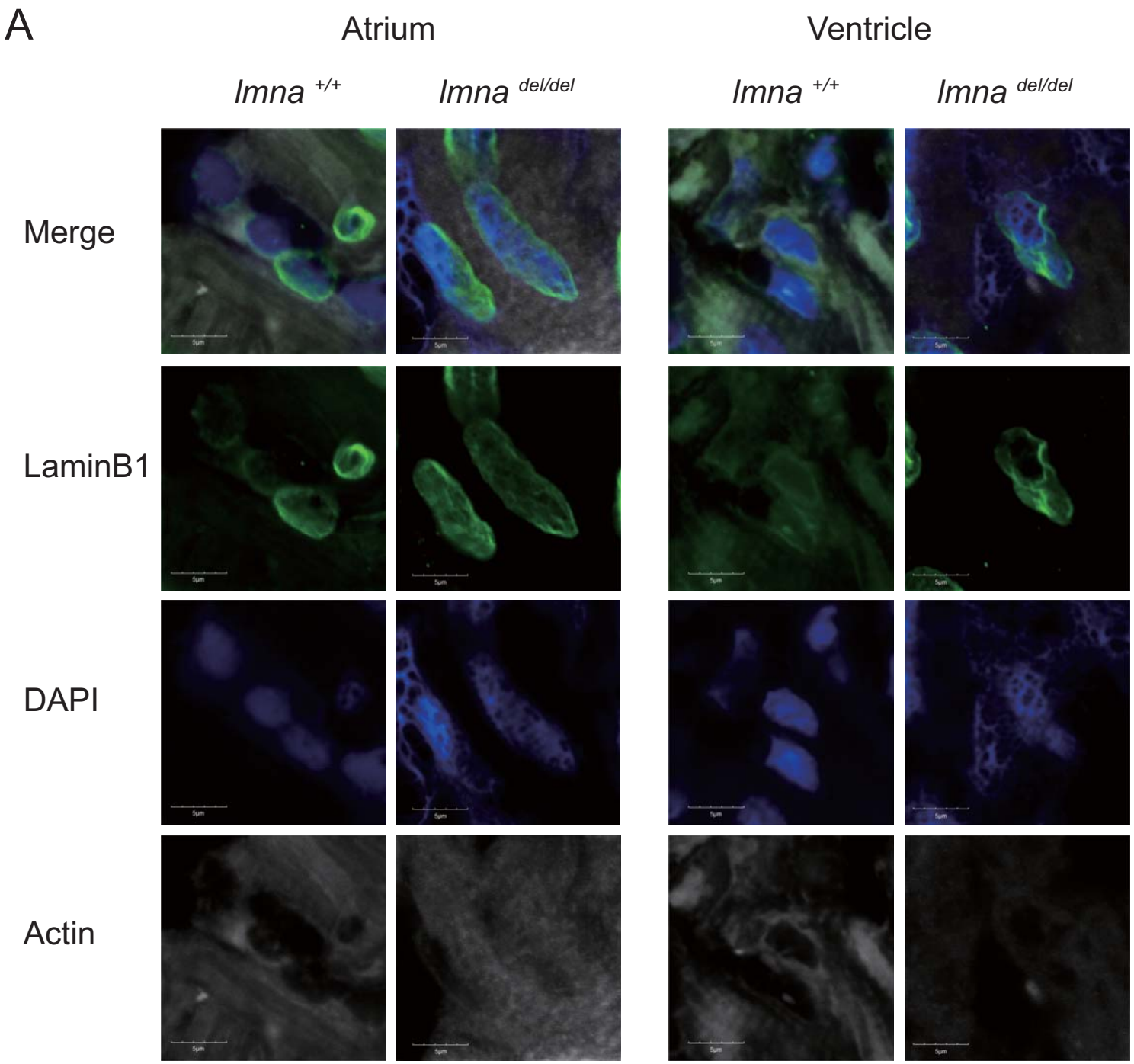
A
Atrium
Ventricle
lmna +/+
lmna del/del
lmna +/+
lmna del/del
Merge
LaminB1
DAPI
Actin

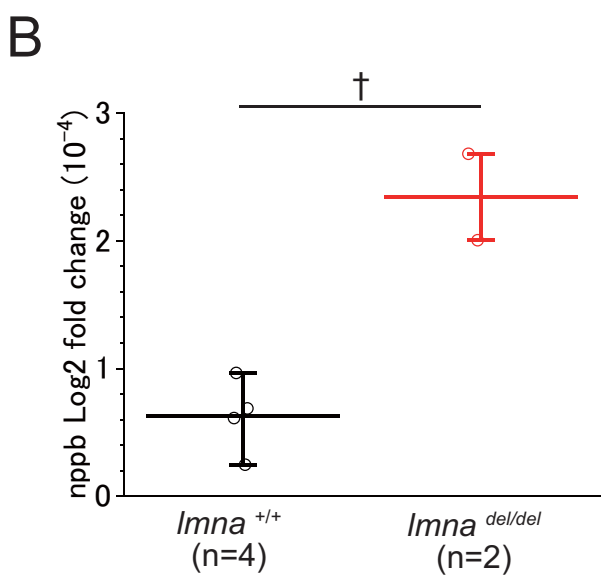
B
†
nppb Log2 fold change (10−4)
3
2
1
0
lmna +/+
(n=4)
lmna del/del
(n=2)

Figure S6

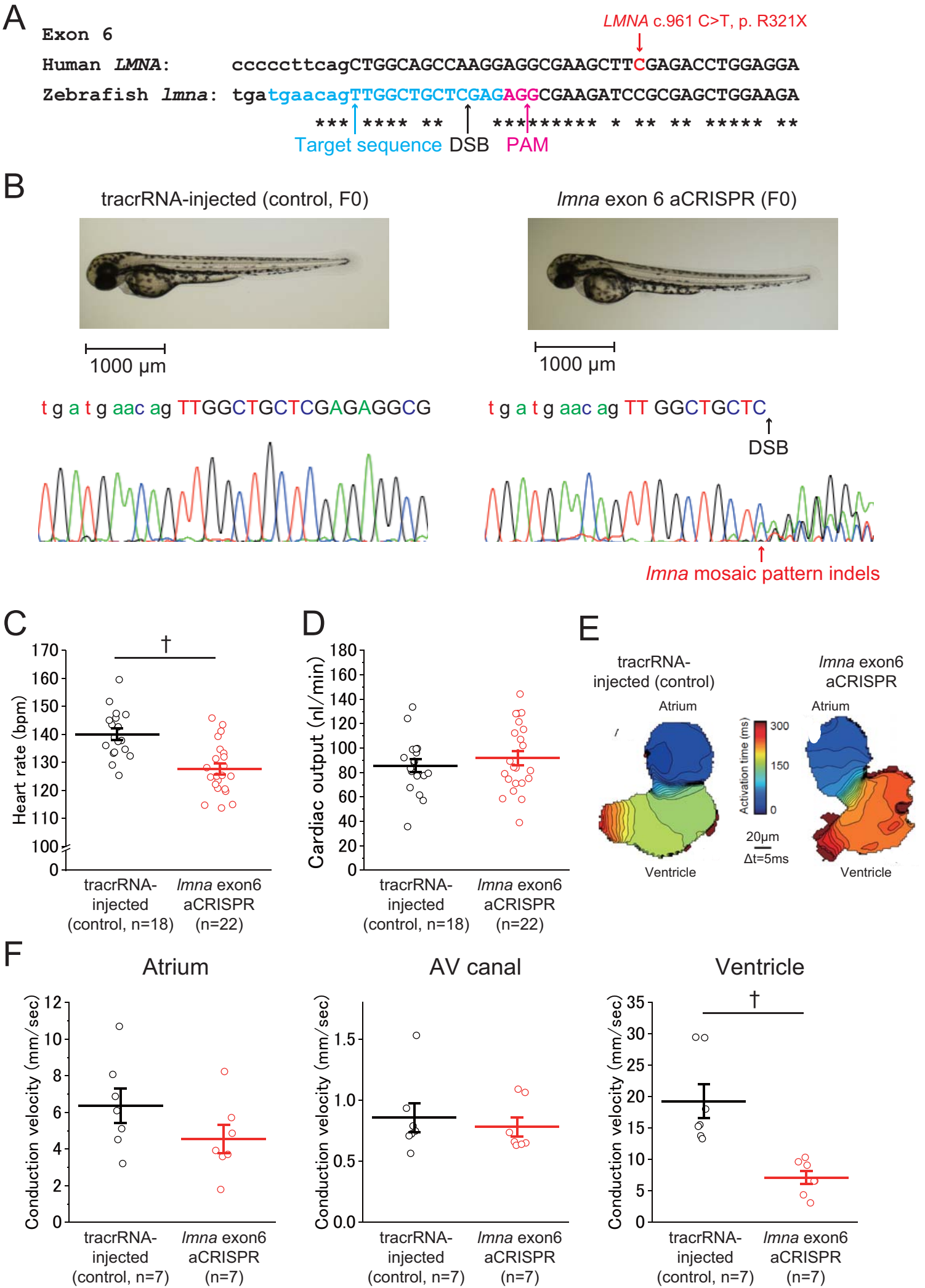
A
Exon 6
LMNA c.961 C>T, p. R321X
Human LMNA: ccccctcagCTGGCAGCCAAGGAGGCGAAGCTTCGAGACCTGGAGGA
Zebrafish lmna: tgatgaacagTTGGCTGCTCGAGAGGCGAAGATCCGCGAGCTGGAAGA
Target sequence
DSB
PAM
B
tracrRNA-injected (control, F0)
lmna exon 6 aCRISPR (F0)
1000 μm
1000 μm
t g a t g aac ag TTGGCTGCTCGAGAGGCG
t g a t g aac ag TT GGCTGCTC
DSB
lmna mosaic pattern indels
C
Heart rate (bpm)
tracrRNA-injected (control, n=18)
lmna exon6 aCRISPR (n=22)
D
Cardiac output (nl/min)
tracrRNA-injected (control, n=18)
lmna exon6 aCRISPR (n=22)
E
tracrRNA-injected (control)
lmna exon6 aCRISPR
Atrium
Ventricle
Activation time (ms)
20μm
Δt=5ms
F
Atrium
AV canal
Ventricle
Conduction velocity (mm/sec)
tracrRNA-injected (control, n=7)
lmna exon6 aCRISPR (n=7)

Figure S7

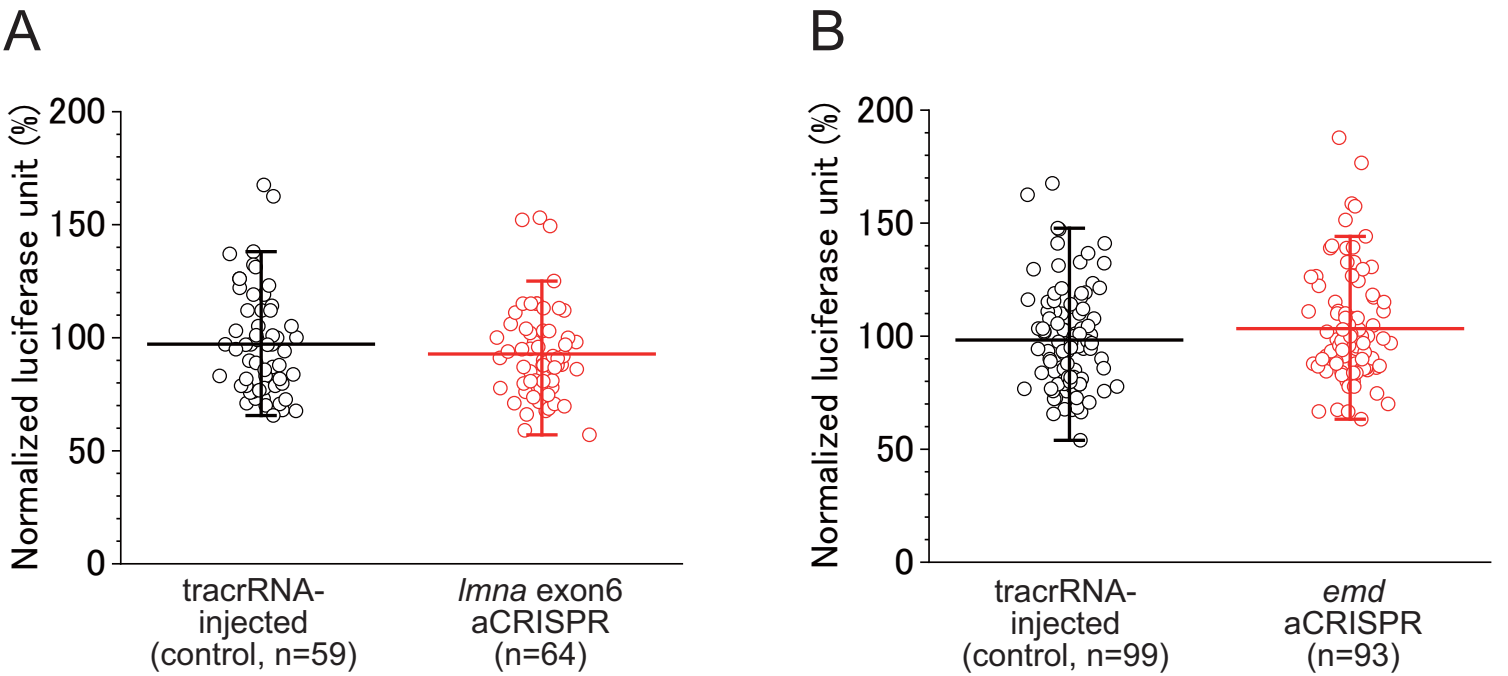
A
Normalized luciferase unit (%)
200
150
100
50
0
tracrRNA-injected (control, n=59)
lmna exon6 aCRISPR (n=64)
B
Normalized luciferase unit (%)
200
150
100
50
0
tracrRNA-injected (control, n=99)
emd aCRISPR (n=93)

Figure S8

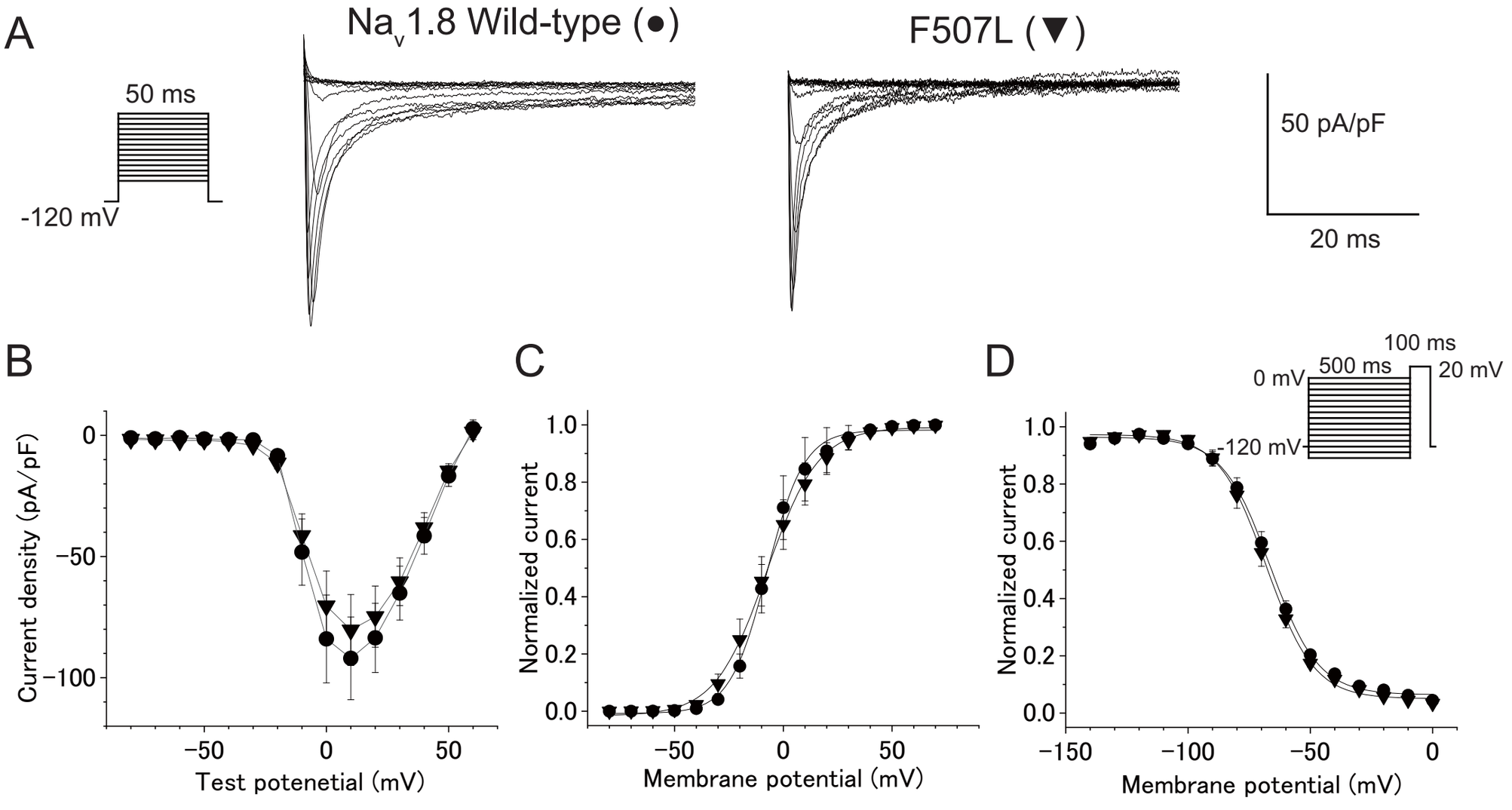
A
Na$_v$1.8 Wild-type (●)
F507L (▼)
50 ms
-120 mV
50 pA/pF
20 ms
B
Current density (pA/pF)
Test potenetial (mV)
C
Normalized current
Membrane potential (mV)
D
100 ms
500 ms
20 mV
0 mV
-120 mV
Normalized current
Membrane potential (mV)

Figure S9

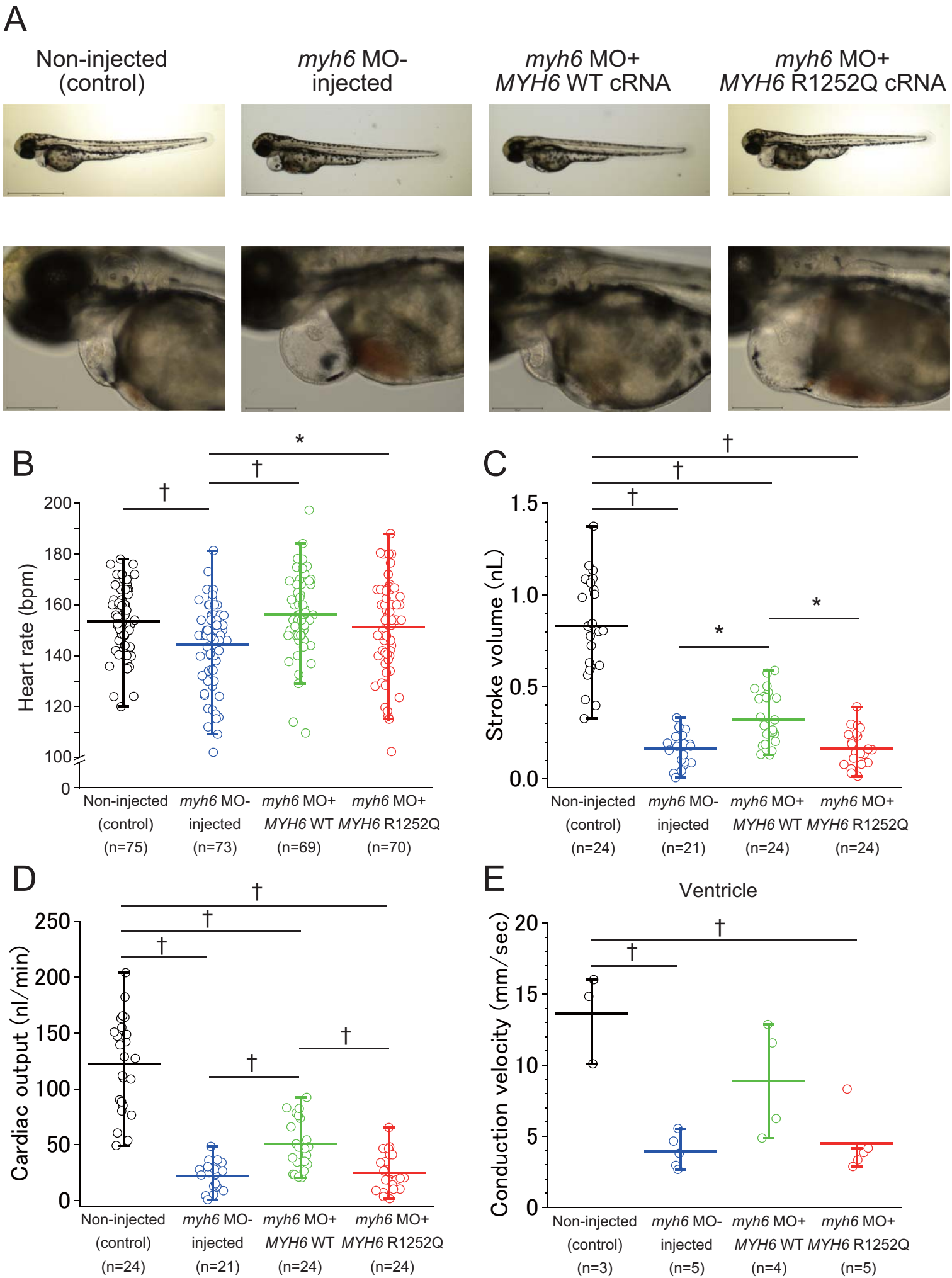
A
Non-injected (control)
myh6 MO-injected
myh6 MO+ MYH6 WT cRNA
myh6 MO+ MYH6 R1252Q cRNA
B
Heart rate (bpm)
200
180
160
140
120
100
0
Non-injected (control) (n=75)
myh6 MO-injected (n=73)
myh6 MO+ MYH6 WT (n=69)
myh6 MO+ MYH6 R1252Q (n=70)
C
Stroke volume (nL)
1.5
1.0
0.5
0.0
Non-injected (control) (n=24)
myh6 MO-injected (n=21)
myh6 MO+ MYH6 WT (n=24)
myh6 MO+ MYH6 R1252Q (n=24)
D
Cardiac output (nl/min)
250
200
150
100
50
0
Non-injected (control) (n=24)
myh6 MO-injected (n=21)
myh6 MO+ MYH6 WT (n=24)
myh6 MO+ MYH6 R1252Q (n=24)
E
Ventricle
Conduction velocity (mm/sec)
20
15
10
5
0
Non-injected (control) (n=3)
myh6 MO-injected (n=5)
myh6 MO+ MYH6 WT (n=4)
myh6 MO+ MYH6 R1252Q (n=5)